Supporting information

Distinguishing among structural ensembles of the GB1 peptide: REMD simulations and NMR experiments

Methods and Materials

1) ^{1}H-NMR spectroscopy

GB1 peptide (Ac-GEWTYDDATKTFTVTE-NH_2) NMR samples were prepared by dissolving lyophilized GB1 peptide directly in a solution of 10 mM phosphate buffer with 10% (v/v) D_2O. NMR sample concentrations were 0.3 to 0.5 mM at pH 7.0. All NMR experiments were performed on a Varian Inova spectrometer operating at a proton frequency of 600 MHz. TOCSY spectra were acquired with an 80 ms DIPSI2 spin lock mixing time and WATERGATE solvent suppression from 278K to 318K with 5 degree increments. 2D NOESY spectra were recorded at 150 ms and 200 ms mixing times with WATERGATE solvent suppression at 278K. Proton chemical shifts are presented in TableS1. The summary of intra-, sequential and long-range NOE connectivities is shown in figure S1.

^{15}N labeled GB1 peptide was expressed in a GST fusion protein and cleaved by AcTEV protease (Invitrogen Inc.). The sequence (ENLYFQGEWTYDDATKTFTVTE) containing an AcTEV protease cutting site (cleaving between Q and G) and GB1 peptide sequence were introduced into pGEX 4T-1 GST expression system. GST-GB1 fusion protein was over-expressed by 1 mM IPTG induction for 4 hours at 37 °C and was purified by FPLC (GE Healthcare, Piscataway, NJ) using a GST affinity column. Pure GST-GB1 fusion protein was digested by AcTEV protease for 3 hours at room temperature; then GST protein, AcTEV protease and GB1 peptide were quickly separated by Superdex-100 size exclusion gel filtration column. 0.5 mM ^{15}N labeled GB1 peptide was prepared for HNHA experiments[1,2]. $^{3}J_{HNHA}$ coupling constants were calculated using the following equation: $I_{cross} / I_{dia} = - \tan^2[\pi J (\Delta1+\Delta2)]$ where I_{cross} and I_{dia} are intensities of cross and diagonal peaks, respectively; $\Delta1$ and $\Delta2$ are 12.57 and 12.49 ms, respectively. The measured $^{3}J_{HNHA}$ coupling constants were listed in Table S1.

2) Computational Details

Replica Exchange Molecular Dynamics Simulations

REMD simulations were performed with 20 replicas run in parallel at the following

20 temperatures: 270, 283, 298, 313, 328, 345, 363, 381, 400, 421, 442, 465, 488, 513, 539, 566, 594, 625, 656, and 690 K - for a total of 10 ns for each replica, with a time step of 1 fs. Transitions between adjacent temperatures were attempted every 250 MD steps using a Metropolis transition probability as detailed in our previous work[3,4]. Configurations were saved prior to every attempted transition, leading to an ensemble at each temperature containing 40,000 structures.

Replica exchange sampling was chosen to generate the peptide ensembles due to the method's ability to sample equilibrium distributions more completely than standard MD sampling. Since we are not focused on dynamics of the solvent, we employed an implicit solvent model, which is a more natural fit to replica exchange simulations than an explicit water model. The implicit solvent model we used, AGBNP[5], is based on a novel pairwise descreening implementation of the generalized Born model and a recently proposed non-polar hydration free energy estimator.

Prediction of HA and HN chemical shifts

SHIFTX was used to generate predicted shifts for all the residues in all 40,000 structures in the ensembles at each simulation temperature. SHIFTX[6] is a hybrid predictive technique that makes use of classical or semi-classical calculations for the effects of ring currents, electric field, hydrogen bond and solvent effects combined with empirical hypersurfaces that capture dihedral angle, sidechain, and nearest neighbor effects that cannot be predicted by classical means. The developers of SHIFTX have estimated correlation coefficients and RMS errors of 0.911 and 0.23 ppm for HA and 0.741 and 0.49 ppm for HN shifts. The lower accuracies for HN shifts may be due to an incomplete quantitative understanding of all of the factors which influence the variability of that shift.

Prediction of J-coupling constants

$J_{HA\text{-}HN}$ coupling constants were calculated from dihedral angles from each residue in each of the peptide structures through a Karplus relationship $J(\theta) = A\cos^2(\theta) + B\cos(\theta) + C$. The values for the parameters A,B, and C were taken from a recent study of coupling constants using ensembles of proteins conducted by Vendruscolo and coworkers[7].

Comparison of predicted HA and HN chemical shifts and J-coupling constants with

experimental values

Mean agreement of the various physical parameters between simulation ensembles and the experimental measurements , as shown in Figure 2 of the communication for HA chemical shifts and in Figures S2 and S3 for HN chemical shifts and J_{HA-HN} coupling constants, were calculated by 1) using SHIFTX(or the Karplus equation) to generate predicted shifts(coupling constants) for all the residues in all 40,000 structures in the ensembles at each simulation temperature, 2) determining the deviation of those shifts(couping constants) from experimental values for those residues, and then 3)taking the RMSD of the means of those distributions. Error bars in these figures were generated by using standard error propagation methods. They are dominated by experimental error, so the error associated with the random coil curve are not perceptible on the scale presented.

Figure S4 shows a comparison of the temperature dependence of the predicted and experimental HN chemical shifts of individual residues. The experimental temperature range, 278-318K is compared to average values from the simulation ensembles for simulation temperatures 381-561K. 381K is matched with experimental low temperature because that is where the HN rmsd plot has its minimum. The temperature dependence of HN chemical shifts over this range of simulation temperatures matches the trends in the experimental temperature dependence of the chemical shifts much more closely than the range starting from the simulation ensemble at 270K (data not shown).

Quantitation of ^{1}H-^{1}H NOEs

^{1}H-^{1}H NOE intensity, because it arises from a dipole-dipole interaction is related to r^{-6} ,where r is the interproton distance. In the fast limit, assuming the members of the ensemble interconvert very rapidly (e.g. a time scale of ~100 ps or faster), NOE intensities scale with distance as $\langle r^{-3} \rangle^2$.[8,9] Therefore, $\langle r^{-3} \rangle$ averaged interproton distances were calculated over the simulation ensembles when comparing NOE derived distances in the simulation ensembles and in the NMR structure of the G-protein.

There is an angular average involved in the exact calculation of the spectral density and the fast motional averaging order parameter.[8,10-13] However, it is common practice in the field, as documented by a long line of papers in the literature[9,14-19], to ignore the angular averaging effects on the calculation of NOEs from molecular dynamics trajectories. The rationale is that the effect of fast angular averaging on NOE intensities is likely to be small compared with that of distance averaging. Even if angular averaging

is not ignored, the argument can be made that the effect is likely to be small because it enters as a root sixth power. The order parameter, S^2, introduced by Lipari and Szabo incorporates the angular term. The effect on NOEs enters the calculation as $(S^2)^{-1/6}$. This means that for example, even for values of the order parameter of S^2 ~0.6, which represent a significant amount of internal angular motion, the order parameter term $(S^2)^{-1/6}$ does not deviate greatly from 1, minimizing the influence of this term on the effective distances extracted from NOE measurements on structural ensembles.

Selection of NOE intensities

All interresidue backbone-backbone NOEs observed in the peptide were included in Figure 3. Backbone-sidechain and sidechain-sidechain NOEs were omitted because of the difficulties in averaging sidechain protons.

residues	H^N	H^α	H^β	H^γ	H^δ	Others	$^3J_{HNHA}$ (Hz)
Gly 41		3.72, 3.82					6.89
Glu 42	8.67	4.40	1.83, 1.97	2.14, 2.20			7.79
Trp 43	8.65	4.91	3.20			$H^{\delta1}$: 7.15 $H^{\varepsilon1}$: 10.10 $H^{\varepsilon3}$: 7.43 $H^{\zeta2/3}$: 7.20, 7.48 H^{η}:7.10	6.73
Thr 44	8.52	4.38	1.20				N/A
Tyr 45	8.56	4.33	2.77, 2.86			$H^{\delta1/2}$: 6.66 $H^{\varepsilon1/2}$: 6.66	8.56
Asp 46	8.17	4.58	2.47, 2.69				8.00
Asp 47	8.44	4.32	2.65				5.84
Ala 48	8.40	4.25	1.47				5.38
Thr 49	7.80	4.25	4.25	1.17			N/A
Lys 50	8.11	4.08	1.86, 1.93	1.35	1.65	H^{ε}:2.97	7.16
Thr 51	7.69	4.47	4.12	1.15			8.92
Phe 52	8.61	4.97	2.99			$H^{\delta1/2}$: 7.21 $H^{\varepsilon1/2}$: 7.32 H^{ζ}: 7.21	6.80
Thr 53	8.63	4.47	4.06	1.15			8.89
Val 54	8.47	4.21	1.78	0.73, 0.81			7.01
Thr 55	8.47	4.38	4.21	1.2			8.12
Glu 56	8.27	4.13	1.90, 2.05	2.21			7.23

Table S1. Proton chemical shift assignments and $^3J_{HNHA}$ measurements at 278K.

Number	*NOE*		*Number*	*NOE*		*Number*	*NOE*
1	47HA-48HN		10	53HA-54HN		19	48HA-50HN
2	45HN-46HN		11	55HA-56HN		20	47HN-49HN
3	47HN-48HN		12	54HA-44HN		21	48HN-50HN
4	48HN-49HN		13	43HA-55HN		22	49HN-51HN
5	51HN-52HN		14	52HA-46HN		23	46HA-51HN
6	55HN-56HN		15	56HA-42HN			
7	45HA-46HN		16	42HN-55HN			
8	46HA-47HN		17	44HN-53HN			
9	50HA-51HN		18	46HA-48HA			

Table S2 A list of the NOEs included in Figure 3 of the paper.

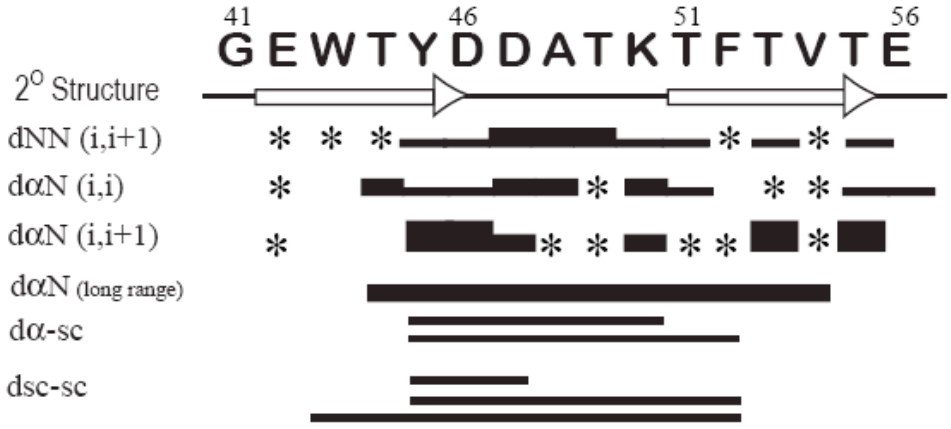

Figure S1. Summary of intra-, sequential and long-range NOE connectivities

Two β-strands are illustrated as arrows according to the protein G B1 structure (PDB: 2GB1). NOE intensities of GB1 peptide were obtained from ^{1}H-^{1}H NOESY experiment. NOEs were classified into three groups, strong, medium and weak, based on the signal strengths and are indicated by the thickness of the lines in this figure. Some weak long-range NOEs (i.e. H^{α} to side-chain proton or side-chain proton to side-chain proton) were observed and presented. Asterisks are NOEs that are overlapped with other peaks and cause uncertainty in categorizing NOE strengths.

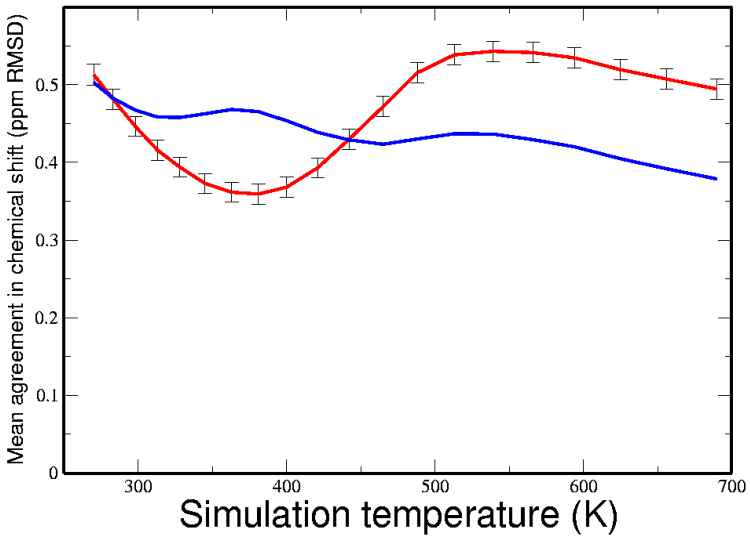

Figure S2 Mean agreement in HN chemical shifts for each simulation ensemble relative to the experimental shifts at 278K(red curve) and random coil(blue curve).

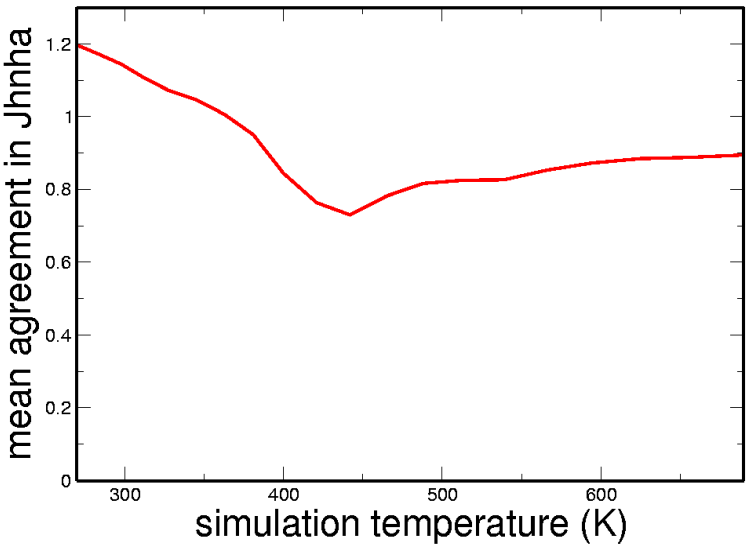

Figure S3 Mean agreement in J_{HAHN} scalar coupling for each simulation ensemble relative to the experimental couplings at 278K.

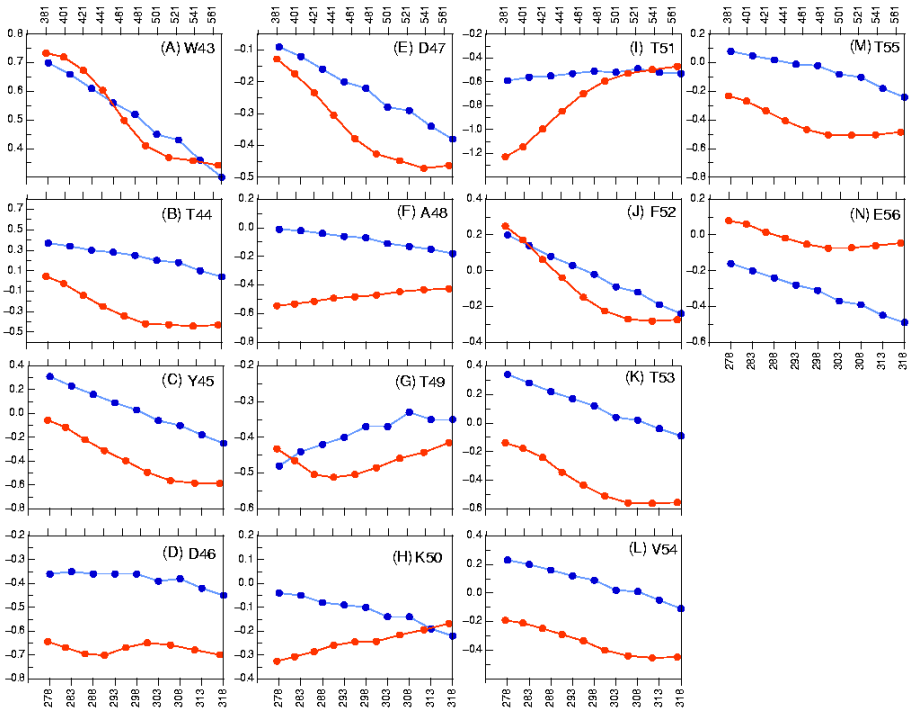

Figure S4 Boxes A to N show the temperature dependent H^N chemical shift deviations of 14 residues (W43 to E56) of GB1 peptide. Experimental NMR data and REMD data calculated from SHIFTX are showing in blue and orange dots in each box, respectively. In each box, Y axis shows the scale of H^N chemical shift deviation (ppm) of the corresponded residue and two X axes are used to present the temperatures of experimental NMR data (278K to 318K, bottom axis) and REMD data (381K to 566K, top axis).

Full Attribution of reference 8 in the manuscript:

(8) J.L. Banks, H.S. Beard, Y. Cao, A.E. Cho, W. Damm, R. Farid, A.K. Felts, T. A. Halgren, D.T. Mainz, J.R. Maple, R. Murphy, D.M. Phillip, M.P. Repasky, L.Y. Zhang, B.J. Berne, R.A. Friesner, E. Gallicchio, and R.M. Levy, *J. Comp. Chem*. 2005, *26*, 1752

References

(1) Vuister, G.W.; Bax, A. *J Am Chem Soc* 1993, 115,7772-7

(2) Grzesiek, S.; Kuboniwa, H.; Hinck, A.P.; Bax, A. *J Am Chem Soc* 1995,117, 5312-5

(3)A.K. Felts, Y. Harano, E. Gallicchio, and R.M. Levy *Proteins* 2004, *56*, 310

(4)M. Andrec, A.K. Felts, E. Gallichio, and R.M. Levy *PNAS* 2005, *102*, 6801

(5) E. Gallicchio and R.M. Levy , *J. Comp. Chem*. 2004, *25*, 479
(6) S. Neal, A.M. Nip, H. Zhang, and D.S. Wishart, *J. Biomol. NMR* 2003, *26*, 215
(7)K. Lindeorff-Larsen, R.B. Best, and M. Vendruscolo *J. Biomol. NMR* 2005, *32*, 273
(8)E.T. Olejniczak, C.M. Dobson, M. Karplus, and R.M. Levy *J. Am. Chem. Soc.* 1984, *106,* 1923
(9)H. Kessler, C. Greisinger, J. Lautz, A. Muller, W.F. van Gunsteren, and H.J. Berendsen *J. Am. Chem. Soc.* 1988, *110*, 3393
(10) J. Tropp *J. Chem. Phys.* 1980, *72*, 6035
(11) G. Lipari and A. Szabo *J. Am. Chem. Soc.* 1982, *104*, 4546
(12) R.M. Levy, M. Karplus and A. McCammon *J. Am. Chem. Soc.* 1981, *103*, 5998
(13) G. Lipari, A. Szabo and R.M. Levy *Nature*, 1982, *300*, 197
(14) B. Richter, J. Gsponer, P. Varnai, X. Salvatella and M. Vendruscolo *J. Biomal NMR* 2007, *37*, 117
(15) W-Y Choy and J.D. Forman-Kay *J. Mol. Biol*. 2001, *308*, 1011
(16) K. L. Constantine, L. Mueller, N.H. Anderson, H. Tong, C.F. Wandler, M.S. Friedrichs, and R.E. Bruccoleri *J. Am. Chem. Soc.* 1995, *117*, 10841
(17) D.A. Pearlman *J. Biomol. NMR* 1994, *4*, 1
(18) A. M. Bonvin and A.T. Brunger *J. Mol. Biol*. 1995, *250*, 80
(19) P. Cuniasse, I. Raynal, A. Yiotakis and V. Dive *J. Am. Chem. Soc*. 1997, *119*, 5239